Predicting copper gallium diselenide and band structure engineering through order-disordered transition

Wenjie Liu, Hanpu Liang, and Yifeng Duan [*]

School of Physics, China University of Mining and Technology, Xuzhou, Jiangsu 221116, China

Zhigang Wu[†]

Department of Physics, Colorado School of Mines, Golden, Colorado 80401, USA

Chalcopyrite $CuGaSe_2$ has been widely studied as a promising light-harvesting material for solar cells, but new stable phases and compounds with other stoichiometries of the Cu-Ga-Se ternary systems could have more desirable properties and their optoelectronic properties could be engineered by controlling the degree of disorder. Employing an *ab initio* evolutionary variable-composition search and Monte Carlo simulations based on the special quasirandom structures, we identified several stable phases of Cu_2Se, Ga_2Se_3, and their alloys $CuGaSe_2$, $CuGa_3Se_5$, $CuGa_5Se_8$, and $Cu_4Ga_2Se_5$ at ambient and high pressures. Computed electronic band structures of these alloys indicate that they are semiconductors with direct band gaps ranging from 0.77 eV of $Cu_4Ga_2Se_5$ to 2.11 eV of $CuGa_3Se_5$. Our results disclose anomalous changes in band gap induced by varying chemical composition and applying high pressure, due to the variation in *p-d* coupling between Se and Cu atoms. Furthermore, the band gap of $CuGaSe_2$ can vary continuously from 1.64 eV for the ordered chalcopyrite structure to 0.23 eV for the fully disordered structure; thus optical absorption spectra in these alloys could be tuned by controlling the synthesis temperature and annealing time, which determine the degree of ordering.

I. INTRODUCTION

As one of the most promising thin-film photovoltaic (PV) materials, $CuGaSe_2$, with the energy conversion efficiency as high as about 20%, has stimulated tremendous research interests [1]. Many methods including doping, vacancy defect, strain engineering, alloying, etc. [2–6], have been proposed to further improve the efficiency. However, such investigations were largely carried out on the basis of the conventional stoichiometry of 1:1 for Cu and Ga, and the crystal symmetry was mostly confined to the chalcopyrite structure. In theory, Cu, Ga and Se could combine in many different ways to form various compounds and structures, though only $CuGa_3Se_5$ and $CuGa_5Se_8$ were reported in experiments so far [7–10], and the quality of measured data was not sufficient to fully solve the crystal structures space group, lattice constants, and atomic positions, which are necessary for band-structure engineering. Furthermore, the structural stability, phase transition, as well as their associated underlying mechanism are still unclear. An open question is whether or not new stable phases or compounds could exist with other chemical compositions, for example, in the copper-rich range. In addition, novel phases and compounds could be synthesized by applying high pressures.

Reliable computational simulations of phase transitions often complement experimental efforts, and they are especially valuable when precise measurements are difficult or not available. For example, several novel phases of the B-C, C-O, Ca-C, Na-Cl, Sn-Se, and W-B systems [11–19] were first predicted theoretically and then discovered experimentally. We aim to fully establish the structures and stoichiometries of copper gallium diselenide, which are expected to provide better optoelectronic performances than chalcopyrite $CuGaSe_2$ [20] due to better band-gap mismatch. In $CuGaSe_2$ the Ga-Se bonds are usually accompanied with the cation-site vacancies [21] influencing their structure stability, phase transition, and optical absorption, which will be investigated as well.

Ordering in a semiconductor alloy could drastically alter its electronic band structure [22–25]; for example, the band gap of $Cs_2AgBiBr_6$ can vary from 0.44 eV with a random cation sublattice to 1.93 eV when the sublattice is fully ordered [25]. Experimentally, disorder might be introduced into the ordered crystal structure at the increased synthesis temperature. Computationally, handling disorder and predicting structural transformation at finite temperature remain very challenging due to the need of a large number of samplings for the disordered systems and the prohibitively expensive calculations of entropy for systems with many atoms in a unit cell [26].

To study configurational disorder in alloys at finite temperatures, we adopt the Monte Carlo simulations with energies evaluated using a cluster expansion effective Hamiltonian [27,28]. This approach was developed to model the order-disorder phenomena when the underlying structure is known. Herein, we will investigate whether one can tune the band gap in $CuGaSe_2$ closer to the optimum value of 1.1–1.5 eV for a single-junction solar cell by rearranging its atomic configuration.

---

[*]yifeng@cumt.edu.cn

[†]zhiwu@mines.edu

In this work, we focus on the fully ordered, partially disordered, and fully disordered alloys of CuGaSe$_2$ using an evolutionary variable-composition search and the Monte Carlo simulations together with the special quasirandom structures (SQS), in order to depict the convex hulls at different pressures for finding novel useful materials desirable optoelectronic properties. Our study provides basic understanding on how Cu, Ga, and Se atoms are combined to form stable materials and on the nature of the chemical reactions responsible for phase transitions induced by pressure, reveals how the alloy energy as well as structure ordering parameters vary quantitatively with respect to temperature, and analyzes the feasibility of band structure engineering through controlling the synthesis temperature and/or annealing time. Thus our results will help stimulate experimental efforts on in-depth investigations of these phenomena to discover new CuGaSe$_2$ structures useful for PV applications.

II. COMPUTATIONAL METHODS

Stable phases in the alloy system were predicted using a first-principles variable-composition evolutionary algorithm as implemented in the USPEX code [29–31]. For each promising composition, the fixed-composition searches were carried out, in combination with structural relaxations and total energy calculations using the density functional theory (DFT [32,33]) within the generalized gradient approximation parameterized by the Perdew, Burke and Ernzerhof (PBE) [34]. The projector augmented wave method [35,36] implemented in the VASP package [37–39] was employed. We used the plane-wave energy cutoff of 450 eV, and Γ-centered **k** meshes of $2\pi \times 0.05\,\text{Å}^{-1}$ resolution for Brillouin zone sampling, ensuring excellent convergence of total energies. During the compositional search, the first and the remaining generations had 200 and 80 structures, respectively, which were produced randomly with up to 32 atoms in a unit cell for the variable-composition search and 42 atoms for the fixed-composition search. The succeeding generations were obtained by applying heredity (35%), soft mutation (15%), and transmutation (15%) operators, respectively. The rest of each generation was created randomly from space groups.

Electronic band structures were calculated using the Heyd-Scuseria-Ernzerhof (HSE) hybrid functional [40] for the equilibrium lattice constants determined by the PBE functional. We found that the HSE functional with the original mixing parameter $a = 0.25$ significantly underestimated the band gaps of Cu$_2$Se, Ga$_2$Se$_3$, and CuGaSe$_2$ at ambient pressure, as seen in Table S1 in the Supplemental Material (hereafter SM) [41], compared with experimental data [42–46] and the PBE and TB-mBJ results. To ensure good accuracy, we increased the mixing parameter a in HSE to be 0.35 and achieved excellent agreement. Thus we adopted $a = 0.35$ for the HSE band structure calculations throughout this work.

The fully disordered solid solution of CuGaSe$_2$ was mimicked by the SQS in the chalcopyrite supercell of 64 and 128 atoms [47], respectively. These configurations were generated by the *mcsqs* utility in the Alloy Theoretic Automated Toolkit (ATAT) [48]. The SQS of 64 and 128 atoms with perfect matchings of atomic correlation functions, were relaxed using the $2 \times 2 \times 2$ and $2 \times 2 \times 1$ **k**-point sampling, respectively.

The partially disordered structures were created using the approach similar to that in generating SQS by finding a supercell structure with its relevant atomic correlation functions closest to the target partially disordered atomic correlation functions.

The order-disorder transition was simulated using the cluster expansion approach as implemented in the *emc*2 utility of the ATAT code [48]. The cluster expansion coefficients were fitted to total energies calculated using the PBEsol functional. The equilibrium structures of the solid solution at high temperatures were determined by the Monte Carlo simulations using a supercell of 201 840 atoms.

III. STRUCTURAL AND ELECTRONIC PROPERTIES

A. Binary compounds

The cubic $Fm\bar{3}m$ [49] and monoclinic $C2/c$ [50] Cu$_2$Se were proposed as the high-temperature and low-temperature phases, respectively. Other phases such as monoclinic $C2/c$, Cm and $C2/m$, orthogonal $Pmn2_1$, tetragonal $P4_32_12$, and orthorhombic $Pca2_1$ [50–53], were also identified for Cu$_2$Se at different conditions. In contrast, Ga$_2$Se$_3$ mainly exists in a monoclinic Cc or an orthorhombic $Imm2$ phase [54,55] based on a defected zinc blende structure. Crystal structures and phonon spectra of these structures for Cu$_2$Se and Ga$_2$Se$_3$ are summarized in Fig. S1 in the SM, with structure parameters listed in Table S2 in the SM. Negative phonon frequencies in Cm Cu$_2$Se for the $Fm\bar{3}m$, $F\bar{4}3m$, Cm, and $Pmn2_1$ structures reveal that these phases can not usually remain dynamically stable at ambient pressure.

We performed the structural search for Cu$_2$Se and Ga$_2$Se$_3$. As pressure increases, Cu$_2$Se and Ga$_2$Se$_3$ share similar symmetries with different space groups. Structures with the successive lowest enthalpies are monoclinic ($P2_1/c$, $C2/m$) and triclinic ($P\bar{1}$) phases for Cu$_2$Se, and monoclinic (Pm, Cc) and triclinic ($P\bar{1}$) phases for Ga$_2$Se$_3$. These structures are plotted in Fig. 1, and their structural parameters are listed in Table S3 in the SM. Phonon spectra of these predicted phases, as shown in Fig. S2 in the SM, display no imaginary modes in the whole Brillouin zone, suggesting that these structures are stable.

The successive phase transitions under high pressures for Cu$_2$Se and Ga$_2$Se$_3$ are summarized in Fig. S3 in the SM. $P2_1c$-Cu$_2$Se undergoes a first-order phase transition to the $C2/m$ phase at $\sim$10 GPa and then a second-order transition to the $P\bar{1}$ phase at $\sim$42 GPa, while Ga$_2$Se$_3$ undergoes a series of first-order phase transitions from Pm to Cc at $\sim$0.25 GPa and then to $P\bar{1}$ at $\sim$9 GPa.

At ambient pressure, the ground state of Cu$_2$Se is predicted to possess the $P2_1/c$ symmetry with a Se-terminated van der Waals (vdW) layered structure, as illustrated in Fig. 1(a). It is energetically preferable to previously reported phases, e.g., the $P2_1/c$ phase is lower in energy than the widely proposed $C2/c$ phase by 13.7 meV/atom. Each Cu atom bonds with three Se atoms, while each Se with six Cu, forming the sp^2 hybridization. The elastic constant $c_{11} = 12$ GPa is much smaller than c_{22} of 109 GPa and c_{33} of 112 GPa, as reported in Table S4 in the SM, owing to the weak vdW interactions between adjacent layers. Since a material with low stiffness usually exhibits large piezoelectric response along the
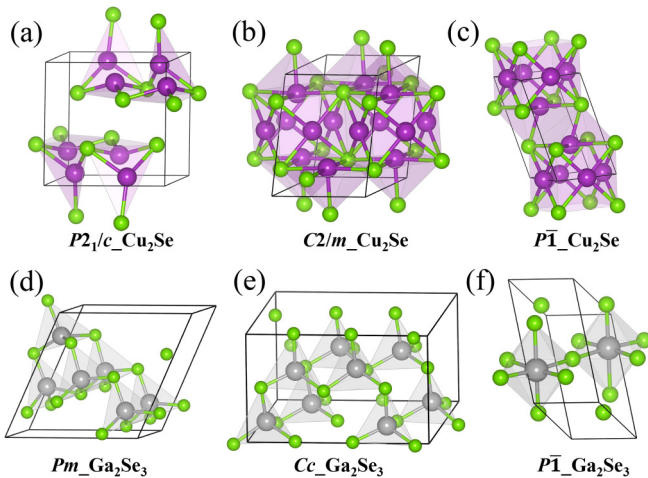
FIG. 1. Crystal structures of Cu_2Se and Ga_2Se_3 at specified pressures. Cu_2Se: (a) $P2_1/c$ at 1 atm, (b) $C2/m$ at 30 GPa, and (c) $P\bar{1}$ at 60 GPa. Ga_2Se_3: (d) Pm at 1 atm, (e) Cc at 0.1 GPa, and (f) $P\bar{1}$ at 60 GPa. The purple, gray, and green spheres represent Cu, Ga, and Se atoms, respectively.

corresponding direction [56,57], $P2_1/c$-Cu_2Se is expected to have strong piezoelectricity along the $\langle 100 \rangle$ direction.

According to the Wyckoff notation, the Cu sites in the $C2/m$-Cu_2Se are classified into Cu ($4i$) and Cu ($4f$). One Cu ($4f$) and four Se ($4i$) atoms form covalent bonds coplanarly, with nearly identical bond lengths and angles of $\sim 90°$. Each Cu ($4i$) atom bonds with five Se ($4i$) atoms, where four covalent bonds are coplanar and the fifth bond is nearly perpendicular to the plane. When pressure is above ~ 42 GPa, the stable structure is predicted to be triclinic $P\bar{1}$, rather than orthorhombic $Pca2_1$ [53], with an enthalpy difference as large as 200 meV/atom at 42 GPa. In the triclinic $P\bar{1}$ phase, the coordination numbers remain unchanged for Cu and Se atoms relative to the $C2/m$ phase, whereas the bonding lengths and angles differ drastically due to the reduced Cu-Cu distance under high pressure. For example, the angle between the out-of-plane and in-plane bonds can be greatly reduced to 68.82° at 60 GPa, in consistency with the change of space group from monoclinic $C2/m$ to triclinic $P\bar{1}$.

We also find a new ground-state phase for Ga_2Se_3, namely, the monoclinic Pm phase, with a total energy lower than the well-known Cc and $Imm2$ phases by 7.06 and 15.06 meV/atom, respectively. The Pm structure shares similar bonding modes with the Cc and $Imm2$ phases. Each Ga atom in the Pm phase is tetrahedrally coordinated by four Se atoms, but 1/3 of cation sites are vacancies because 1/3 of Se atoms are coordinated by two Ga atoms, while the remaining Se atoms are bonding with three Ga atoms. It is well known that in the Cc structure the vacancies are located zigzaggedly, while in the Pm structure, the vacancy sites form straight lines and three neighboring "lines" stand side by side to loosely form a triangle, as viewed along the $\langle 010 \rangle$ direction. Once pressure is above ~ 9 GPa, another Se-terminated vdW layered $P\bar{1}$ structure becomes stable, whose bonding is somewhat similar to that of the rocksalt structure. Each Ga and Se ($1f$) atom is sixfold coordinated, but the coordination number is three for Se ($2i$) atoms located at the surface of each layer.
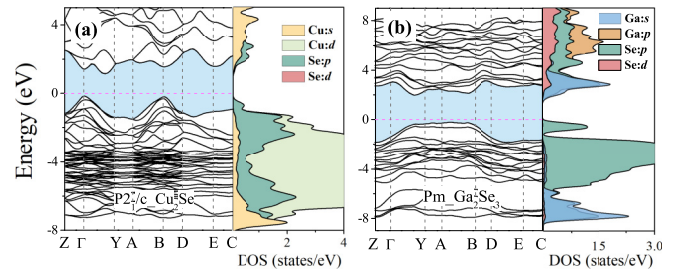

FIG. 2. Electronic band structures and DOS of Cu_2Se and Ga_2Se_3 at ambient pressure using the HSE functional.

Figure 2 summarizes the calculated electronic band structures and density of states (DOS) for the predicted phases of Cu_2Se and Ga_2Se_3 at ambient pressure, which are semiconductors with indirect band gaps. The band structures and DOS for high-pressure phases plotted in Fig. S4 in the SM, suggest that $C2/m$-Cu_2Se, $P\bar{1}$-Cu_2Se, and $P\bar{1}$-Ga_2Se_3 are metallic, but Cc-Ga_2Se_3 is semiconducting. We find that when the coordination number of cation is three or four, Cu_2Se and Ga_2Se_3 are semiconductors; once this number increases above four, these materials become metallic.

As indicated by the calculated DOS (Fig. 2), the $3d$-orbital binding energy of Ga atom is ~ 18 eV, much larger than that of ~ 5 eV of Cu atom, and the valence band maximum (VBM) is mainly occupied by the Se p states in Cu_2Se and Ga_2Se_3. Cu_2Se has a much stronger p-d coupling than that in Ga_2Se_3, leading to a smaller band gap (E_g) of 1.26 eV in Cu_2Se than that of 2.16 eV in Ga_2Se_3, because the p-d repulsion can push the VBM up and then reduce the band gap [58,59]. Therefore, the electronic and optical properties of ternary alloys are determined largely by the coupling between Cu $3d$ and Se $4p$ states, not by the interactions between Ga $3d$ and Se $4p$ states. This can be further verified by effective mass. Compared with Ga_2Se_3, Cu_2Se has more dispersive bands near the VBM, indicating smaller effective masses of electrons.

B. Ternary compounds

We calculated the complete convex hull diagrams using the following expression

$$\Delta H = H[(Cu_2Se)_{(1-x)}(Ga_2Se_3)_x] \\ - (1-x)H(Cu_2Se) - xH(Ga_2Se_3) \quad (1)$$

to identify stable and metastable structures and stoichiometries, as plotted in Fig. 3. Convex hull construction provides a global view of the relative stabilities of structures and stoichiometries for binary, ternary, quaternary systems, etc. By definition, a thermodynamically stable phase has a lower enthalpy (or, more generally, Gibbs free energy) than any other phases or phase assemblage of the same composition. A structure on the convex hull is thermodynamically stable, while a structure above the hull is metastable.

Figure 3(a) plots the formation enthalpies for ternary alloys at ambient pressure. The formation energies of conventional alloys are usually positive and follow parabolic convex curves due to large strain energy. However, in this Cu-Ga-Se ternary system, the formation energy curve is concave, and the
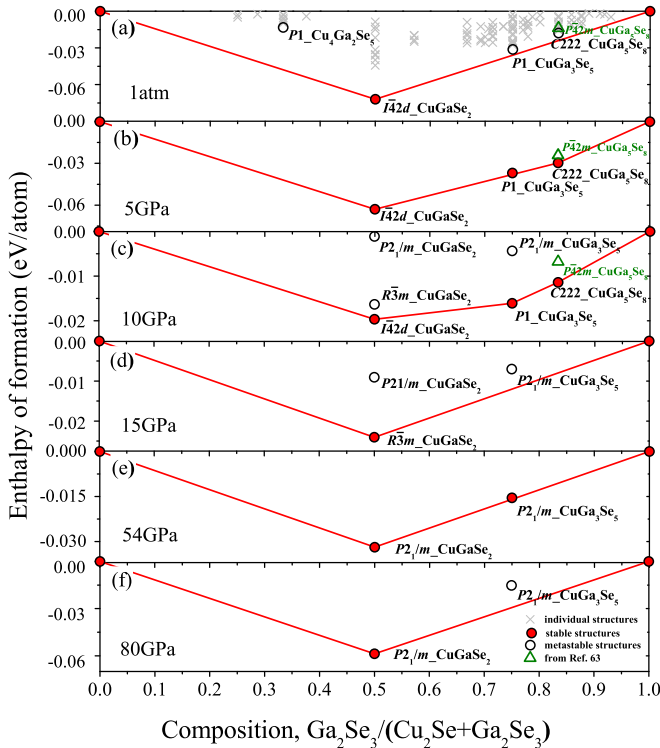
FIG. 3. Thermodynamic convex hulls of ternary alloys at different pressures. Filled circles are stable phases, open circles are metastable, and open triangles are phases from Ref. [63].

thermodynamically stable structure exists at chemical composition of 50%, i.e., chalcopyrite $CuGaSe_2$ ($I\bar{4}2d$), due to the fact that Coulomb interactions lower the formation energy and thus the ordered structures are preferred. Since the effective Coulomb interaction is relatively short ranged, the search for stable phases is, in fact, to find the minimum atomic correlation function $\bar{\Pi}_{(2,1)}$ for the nearest neighbor "figure" in view of cluster expansion theory [60,61]. The Coulomb energy gain is proportional to $\langle\bar{\Pi}_{(2,1)}\rangle_{min}$-$\langle\bar{\Pi}_{(2,1)}\rangle_{random}$ and the formation energy minimum is located at composition of 0.5 [61].

$CuGa_3Se_5$, $CuGa_5Se_8$ and $Cu_4Ga_2Se_5$ of the $P1$, $C222$ and $P1$ symmetries remain metastable at ambient pressure, and there are no stable phases existing for the ternary system when the zero-point energy is taken into account (Fig. S5 in the SM). $CuGa_3Se_5$ is most likely to become stable, which is above the convex hull only by 4.75 meV/atom, whereas $CuGa_5Se_8$ and $Cu_4Ga_2Se_5$ are above the hull by 6.23 and 34.69 meV/atom, respectively. This metastability does not preclude these materials from experimental synthesis, which is supported by the fact that the observed metastable phases are usually within 0.1-0.2 eV/atom above the ground state [62]. According to the inorganic crystal structure database, 20% of experimentally synthesized materials are metastable, some of which even have high positive formation enthalpies. For example, the $P\bar{4}2m$ phase of $CuGa_5Se_8$ is higher in energy than the $C222$ phase by 3.83 meV/atom, and it has been confirmed experimentally [63]. Therefore, it is possible to synthesize these gallium-rich phases at ambient pressure.

As pressure increases near 5 GPa, $P1$-$CuGa_3Se_5$ and $C222$-$CuGa_5Se_8$ become thermodynamically stable successively [Fig. 3(b)], consistent with Sun *et al.* [62]. As pressure further increases to 10 GPa, $R\bar{3}m$-$CuGaSe_2$, $P2_1/m$-$CuGaSe_2$, and $P2_1/m$-$CuGa_3Se_5$ become metastable [Fig. 3(c)]. Figures 3(d)–3(f) indicate that stable $CuGaSe_2$ transforms from the $I\bar{4}2d$ phase to the $R\bar{3}m$ phase at ~11 GPa, and then to the $P2_1/m$ phase above ~42 GPa. When pressure is about 54 GPa, $P2_1/m$-$CuGa_3Se_5$ becomes close to the convex and reaches the marginal stability.

As discussed above, the stable or metastable phases of the ternary system at ambient pressure can be understood by the formation of covalent bonds. Specifically, the Ga-Se bonding is more covalent than the Cu-Se bonding, due to the increment of electronegativity from Cu to Ga and to Se atom; therefore Ga-Se bonds are easier to form than Cu-Se bonds, leading to stable phases existing mainly in the Ga-rich range. Moreover, since the Ga atom is larger in size than the Cu atom, mixing the Ga atom into the alloy structure enlarges the lattice constants and increases the strain energy and thus raises the formation energy. Thus the increase in Ga composition lifts the energy barriers for Ga-rich structure to be stable. In other words, in the Ga-rich range, the compounds with higher Ga composition are expected to have fewer stable phases, consistent with our current finding that $CuGaSe_2$ has three stable phases, $CuGa_3Se_5$ has two, while $CuGa_5Se_8$ has only one.

The absence of any imaginary frequency phonon modes in the whole Brillouin zone suggests the dynamical stability of $I\bar{4}2d$-, $R\bar{3}m$-, and $P2_1/m$-$CuGaSe_2$, $P1$- and $P2_1/m$-$CuGa_3Se_5$, $C222$- and $P\bar{4}2m$-$CuGa_5Se_8$, and $P1$-$Cu_4Ga_2Se_5$ at specified pressures (Fig. S6 in the SM, structural parameters are summarized in Table I). The elastic constants for stable phases at ambient pressure were calculated, as listed in Table S4 in the SM, and the relevant parameters including bulk modulus, shear modulus, Young's modulus, Poisson ratio, and Vickers hardness, are summarized in Table S5 in the SM. The elastic constants satisfy the Born stability criteria [64]. Based on these data, we constructed the pressure-composition phase diagram (Fig. 4), which allows one to identify materials with an optimal combination of these properties.

Figure 5 plots crystal structures of $CuGaSe_2$, $CuGa_3Se_5$, $CuGa_5Se_8$, and $Cu_4Ga_2Se_5$ under high pressures. Our results of Ga_2Se_3 and $CuGaSe_2$ reveal that increasing Ga composition introduces the vacancies, which exist only when Ga composition is above 50%. At ambient pressure, although the tetrahedral bonding is preferred, the cation-site vacancies lead to anomalous bonding modes for Se atoms. In $P1$-$CuGa_3Se_5$, 3/5 of Se atoms are coordinated by two Ga and one Cu atoms, 1/5 by three Ga and one Cu atoms, and 1/5 by three Ga atoms. According to the number of dangling bonds, 1/5 of cation sites are vacancies. When the Ga composition increases to 5/6 in $CuGa_5Se_8$, the vacancy proportion is enhanced to 1/4: half of Se atoms bond with three Ga atoms, and half with two Ga and one Cu atoms. In $CuGa_5Se_8$ system, the vacancies form a straight line in the $C222$ phase along the $\langle001\rangle$ direction, while straight-line and zigzag-line vacancies coexist in the $P\bar{4}2m$ phase. In $P1$-$Cu_4Ga_2Se_5$, Cu atoms have unexpected dangling bonds, and half of Cu atoms bond with three Se atoms with bonding angle of ~62°. The bonding

TABLE I. Structure parameters of stable ternary alloys at specified ranges of pressure.

	Structure	Parameters(Å,°)	Atom	x	y	z	P(GPa)
$CuGaSe_2$	$I\bar{4}2d$	a=b=5.67	Cu(4a)	0.00	0.50	0.25	0.0001
		c=11.26	Ga(4b)	0.50	0.50	0.00	
		$\alpha=\beta=\gamma$=90	Se(8d)	0.75	0.75	0.125	
	$R\bar{3}m$	a=b=3.61	Cu(3b)	0.33	0.67	0.17	11
		c=17.73,γ=120	Ga(3a)	0.67	0.33	0.33	
		$\alpha=\beta$=90	Se(6c)	0.67	0.33	0.09	
	$P2_1/m$	a=6.96,b=4.39	Cu(2e)	0.18	0.75	0.36	55
		c=3.47	Ga(2e)	0.68	0.75	0.37	
		$\alpha=\gamma$=90	Se(2e)	0.41	0.75	0.84	
		β=85.34	Se(2e)	0.08	0.25	0.18	
$CuGa_3Se_5$	$P1$	a=5.60,b=6.89	Cu(1a)	0.09	0.43	0.74	0.0001
		c=6.82	Ga(1a)	0.74	0.02	0.54	
		$\alpha=98.96$	Ga(1a)	0.92	0.23	0.15	
		β=114.14	Ga(1a)	0.51	0.81	0.94	
		γ=66.07	Se(1a)	0.56	0.12	0.83	
			Se(1a)	0.98	0.53	0.05	
			Se(1a)	0.74	0.34	0.43	
			Se(1a)	0.18	0.71	0.63	
			Se(1a)	0.37	0.91	0.25	
	$P2_1/m$	a=3.59,b=6.22	Cu(2e)	0.75	0.08	0.39	15
		c=13.97	Ga(2e)	0.75	0.75	0.83	
		$\beta=\gamma$=90	Ga(2e)	0.75	0.75	0.17	
		α=90.14	Ga(2e)	0.25	0.58	0.40	
			Se(2e)	0.75	0.08	0.08	
			Se(2e)	0.75	0.76	0.50	
			Se(2e)	0.25	0.59	0.71	
			Se(2e)	0.25	0.92	0.29	
			Se(2e)	0.75	0.42	0.92	
$CuGa_5Se_8$	$C222$	a=11.05,b=11.29	Cu(2b)	0.00	0.50	0.00	0.0001
		c=5.52	Ga(4h)	0.00	0.75	0.50	
		$\alpha=\beta=\gamma$=90	Ga(4k)	0.25	0.25	0.98	
			Ga(2a)	0.00	0.00	0.00	
			Se(8l)	0.13	0.38	0.73	
			Se(8l)	0.86	0.12	0.74	
	$P\bar{4}2/m$	a=b=5.53,	Cu(1b)	0.50	0.50	0.50	0.0001
		c=11.32	Ga(1a)	0.00	0.00	0.00	
		$\alpha=\beta=\gamma$=90	Ga(4m)	0.5	0.00	0.25	
			Se(4n)	0.73	0.27	0.12	
			Se(4n)	0.76	0.24	0.62	
$Cu_4Ga_2Se_5$	$P1$	a=4.02,b=5.74	Cu(1a)	0.85	0.57	0.02	0.0001
		c=10.78	Cu(1a)	0.60	0.69	0.52	
		$\alpha=\gamma$=90	Cu(1a)	0.65	0.34	0.63	
		β=62.2	Cu(1a)	0.22	0.00	0.82	
			Ga(1a)	0.25	0.97	0.83	
			Ga(1a)	0.44	0.17	0.22	
			Se(1a)	0.35	0.80	0.02	
			Se(1a)	0.75	0.23	0.83	
			Se(1a)	0.94	0.43	0.22	
			Se(1a)	0.54	0.03	0.42	
			Se(1a)	0.15	0.61	0.64	

disorder enlarges the formation energy, and this phase only remains stable in a narrow range of pressure.

For $R\bar{3}m$- and $P2_1/m$-CuGaSe$_2$, the coordination number increases to six. In $R\bar{3}m$ structure, each Se atom is coordinated by three adjacent Cu and three adjacent Ga atoms with different angles due to slight difference in bonding lengths. At 11 GPa, the Cu-Se-Cu bonding angle is 91.4°, the Ga-Se-Ga bonding angle is 88.6°, and the Ga-Se-Cu bonding angle is 90°. In $P2_1/m$ structure, the Cu-Ga distance is reduced greatly under high pressure, leading to abrupt changes in bonding angles. For instance, at 60 GPa, the Ga-Se-Cu bonding angle is reduced to 66.7°. $P2_1/m$-CuGa$_3$Se$_5$ shows a Se-terminated
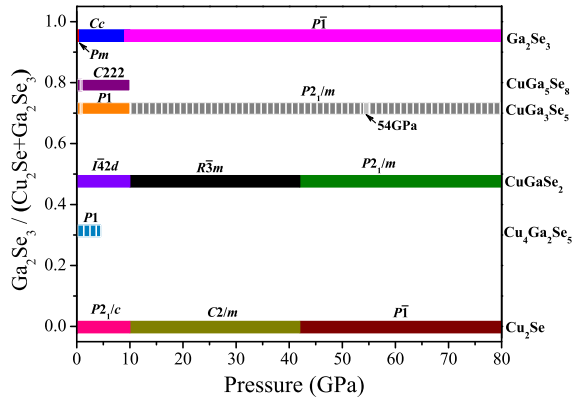
FIG. 4. Pressure-composition phase diagram of Cu_2Se, Ga_2Se_3 and their alloys. The solid (dashed) lines represent the stable (metastable) phases.

vdW layered structure due to the special mode of vacancies. These two vdW layered materials share similar bonding characteristics, including the coordination number, bonding angle, etc. We plotted the electronic band structures in Fig. S7 in the SM, showing that $R\bar{3}m$-$CuGaSe_2$, $P2_1/m$-$CuGaSe_2$, and $P2_1/m$-$CuGa_3Se_5$ are all metallic, consistent with the conclusion drawn for Cu_2Se and Ga_2Se_3—when the coordination number of Cu or Ga atom is above four, a semiconductor-to-metal transition occurs.

Figure 6 summarizes electronic band structures and DOS of $I\bar{4}2d$-$CuGaSe_2$, $P1$-$CuGa_3Se_5$, $C222$-$CuGa_5Se_8$, and $P1$-$Cu_4Ga_2Se_5$ at ambient pressure, indicating that these materials are direct band gap semiconductors with the VBM and conduction band minimum (CBM) at the Γ point. The CBM states mainly originate from the Ga s and Se p states. The Cu s state exists at the CBM in Cu_2Se, but not in alloys. This is because the atomic energy level of Cu s state is higher than that of Ga s state; for instance, the difference is 3.20 eV

in ground-state $CuGaSe_2$. Furthermore, as Ga composition increases, the Ga s state contributes more to the CBM states of alloys.

Figure 6 also indicates that the atomic energy level of Cu d states is significantly above that of Ga d states. In view of p-d repulsion, the Cu d states play a more important role in determining the VBM than the Ga d states. Specifically the strong intersite hybridization between Cu d (t_{2g} orbitals [65]) and Se p states forms antibonding states between -3.0 and 0 eV and bonding states between -5.5 and -4 eV. The Cu d states around from -4.0 to -3.0 eV, namely, the e_g orbitals [65], form nonbonding states with flat bands. In compounds with different stoichiometries, the binding energy of Cu d electrons is slightly shifted. Our results further reveal that such binding energy is sensitive to pressure. Therefore, it is possible to precisely tune E_g by controlling Ga composition or pressure.

At ambient pressure, since Ga_2Se_3 has a larger E_g of 2.16 eV than that of 1.26 eV in Cu_2Se, E_g is expected to become bigger for larger Ga composition due to the weakened p-d coupling between Se and Cu atoms lowering the VBM. While this is true going from $Cu_4Ga_2Se_5$ ($E_g = 0.77$ eV) to $CuGaSe_2$ (1.64 eV) and to $CuGa_3Se_5$ (2.11 eV), $Cu_4Ga_2Se_5$ has an anomalously smaller E_g than that of Cu_2Se, and $CuGa_5Se_8$ has a smaller E_g of 1.87 eV than $CuGa_3Se_5$, as illustrated in Fig. 7(a) (starting points). In $Cu_4Ga_2Se_5$, the p-d hybridization is weaker than in Cu_2Se, which tends to enhance band gap, while the CBM states mainly originate from Ga s state, not from Cu s state as in Cu_2Se. Figure 7(b) indicates that the energy level of Ga s state is much lower than that of Cu s state, eventually resulting in the reduction of E_g. Figure 7(c) shows that although the binding energy of Cu d states is comparable in $CuGa_3Se_5$ and $CuGa_5Se_8$, the DOS is higher in $CuGa_5Se_8$ than in $CuGa_3Se_5$ due to the associated crystal symmetries, implying a stronger p-d hybridization in $CuGa_5Se_8$, which leads to a smaller E_g in $CuGa_5Se_8$ than in $CuGa_3Se_5$.

Band gap in compounds can often be reduced by applying high pressure irrespective of whether the d orbitals are occupied or not [66,67]. In practice, it is also possible to enlarge E_g by adjusting the binding energy of Cu d states through pressure. Figure 7(a) suggests that, as pressure increases, E_g increases monotonously in $Cu_4Ga_2Se_5$, $CuGaSe_2$, and $CuGa_3Se_5$. Figure S8 in the SM indicates that the Cu-d binding energies of these semiconductors are enhanced by pressure, and the weakened p-d coupling leads to the rise of E_g. Figure 7(d) suggests that, initially as pressure increases, the weakening of p-d coupling results in the increase in E_g, but, as pressure further increases, this Cu-d DOS becomes so weak that the strength of p-d coupling is no longer the decisive factor determining the evolution of E_g with respect to pressure, and then E_g will be reduced by pressure. This conclusion is consistent with our results plotted in Fig. 7(a), where E_g of $CuGa_5Se_8$ is enlarged initially and then suppressed by pressure at a critical value of ~ 8 GPa.

IV. ORDERED-DISORDERED TRANSITION

In this session, we study the engineering of optical properties by controlling the ordering parameter in $CuGaSe_2$, which
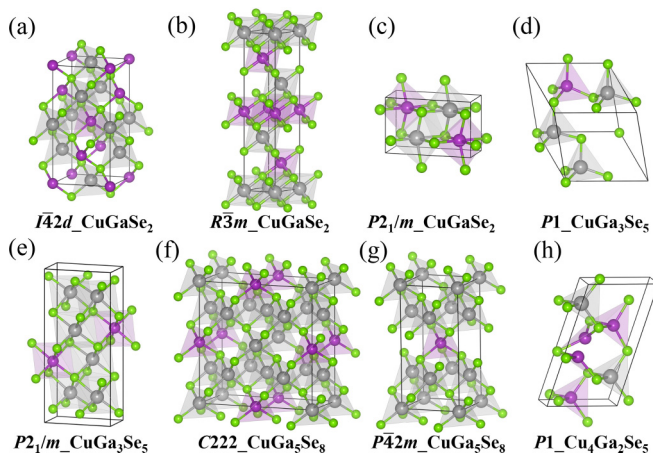

FIG. 5. Crystal structures of stable alloys at specified pressures. $CuGaSe_2$: (a) $I\bar{4}2d$ at 1 atm, (b) $R\bar{3}m$ at 11 GPa, and (c) $P2_1/m$ at 55 GPa. $CuGa_3Se_5$: (d) $P1$ at 1 atm and (e) $P2_1/m$ at 12 GPa. $CuGa_5Se_8$: (f) $C222$ at 1 atm and (g) $P\bar{4}2m$ at 1 atm. $Cu_4Ga_2Se_5$: (h) $P1$ at 1 atm. The purple, gray, and green spheres represent Cu, Ga, and Se atoms, respectively.
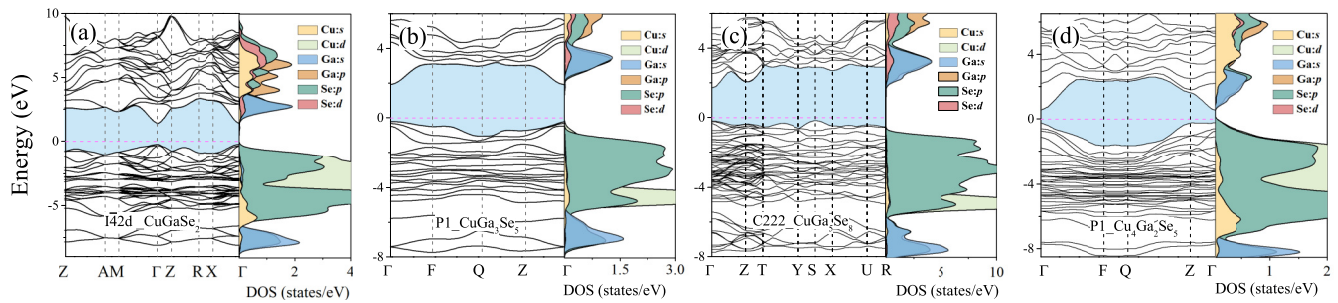
FIG. 6. HSE band structures and DOS of stable ternary alloys at ambient pressure.

can be realized by controlling the synthesis temperature or annealing time. We focus on the optical absorptions because experimental E_g are usually obtained from optical measurements. First, we systematically investigated the optical transitions of ordered chalcopyrite CuGaSe₂. The joint electronic band structure is plotted in Fig. 8(a), displaying the energy differences between first conduction band and twenty top valence bands. We also calculated the imaginary part of the dielectric function ($\epsilon_{xx} = \epsilon_{yy}$ and ϵ_{zz}) within the one-electron theory (i.e., the exciton effects are not included), as shown in Fig. 8(b). There are slight dislocations between ϵ_{xx} and ϵ_{zz}, with the energy difference of merely ∼0.10 eV between the first absorption peaks at ∼1.65 eV, due to the reduced crystal symmetry in the chalcopyrite structure derived from the zinc blende structure. Here the first absorption peaks of ϵ_{zz} and ϵ_{xx} arise from the transitions from the first valence band and the twofold degenerate (second and third) valence bands to the first conduction band at the Γ point, respectively.

To study the phase transition from ordered to disordered states, the relationship between energy and ordering parameter has been established on the basis of cluster expansion theory [25,68] as follows

$$E(\sigma) = E_R + \sum_{km} J_{km} \bar{\Pi}_{km}. \qquad (2)$$

E(σ) and E$_R$ are the total energies of the structures of the configuration σ and of the fully disordered solid solution, respectively. J_{km} is the effective interaction within clusters consisting of k atoms separated by m neighbors, and $\bar{\Pi}_{km}$ is the average of the atomic correlation functions of cluster (k, m). Here k represents the number of vertices in the polyhedron

figures such as pairs ($k = 2$), triangles ($k = 3$), and tetragons ($k = 4$) and m represents the mth-neighbored distance. In Ising models, each cation site i can be assigned to a spin variable S_i, which is +1 if it is occupied by Cu⁺ and −1 if by Ga³⁺. The $\bar{\Pi}_{km}$ is the product of S_i. For an ordered alloy, $\bar{\Pi}_{21} = -1$, whereas in perfectly disordered structure, $\bar{\Pi}_{km} = 0$ for all figures.

Since the atomic interactions are relatively short ranged, the $\bar{\Pi}_{km}$ can be safely restricted to the pairs up to the fourth neighbors. Equation (2) is simplified as

$$E(\sigma) \doteq E_R + J_{21}\bar{\Pi}_{21} + J_{22}\bar{\Pi}_{22} + J_{23}\bar{\Pi}_{23} + J_{24}\bar{\Pi}_{24}. \qquad (3)$$

The atomic correlation function $\bar{\Pi}_{21}$ has the dominant effect on the energy and phase transition [25]. This is also true in CuGaSe₂, for instance, $\bar{\Pi}_{21}$ of 75.2 meV is much larger than $\bar{\Pi}_{22}$ of 9.11 meV. Thereby $\bar{\Pi}_{21}$ can be used as an ordering parameter varying from 0 for the fully disordered structure to −1 for the ordered chalcopyrite structure.

We have carried out Monte Carlo simulations using a large supercell of 201 840 atoms at various temperatures. Figure 9 plots the excess energy and the correlation functions $\bar{\Pi}_{2m}$ up to the fourth neighbor as functions of temperature. When temperature is increased from 0 to 700 K, the energy per cation site and $\bar{\Pi}_{2m}$ barely change, indicating that the structure remains ordered under 700 K. Then energy rises slowly as temperature is further increased to 1800 K. However, in the range of 1800 K to 2700 K, energy and $\bar{\Pi}_{2m}$ rise sharply, suggesting an ordered-to-disordered phase transition. After the phase transition, $\bar{\Pi}_{2m}$ approach zero, the value for fully disordered structure.
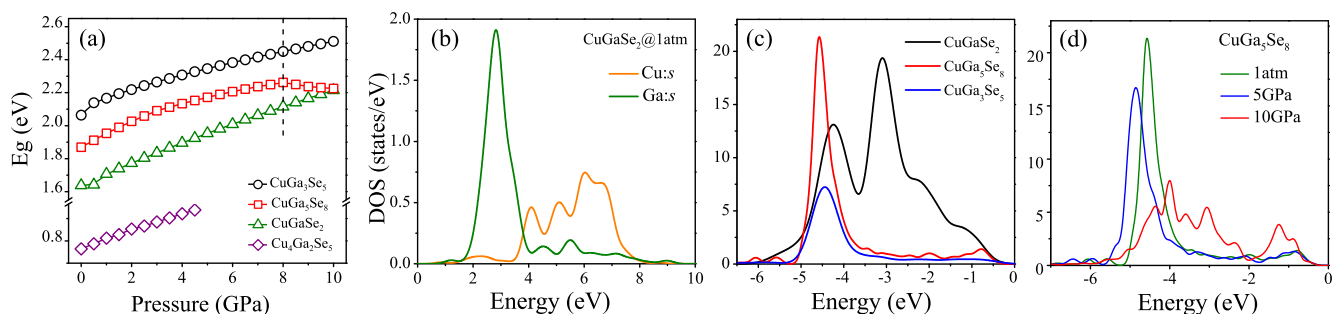
FIG. 7. (a) HSE E_g as functions of pressure for stable alloys. (b) Detailed Cu-s and Ga-s DOS above the E_F of chalcopyrite CuGaSe₂. (c) Cu-d DOS below the E_F of CuGaSe₂, CuGa₃Se₅, and CuGa₅Se₈ at ambient conditions. (d) Cu-d DOS below the E_F of CuGa₅Se₈ at special pressures. The calculations are performed within HSE functional, and the VBM is set to zero in each panel.
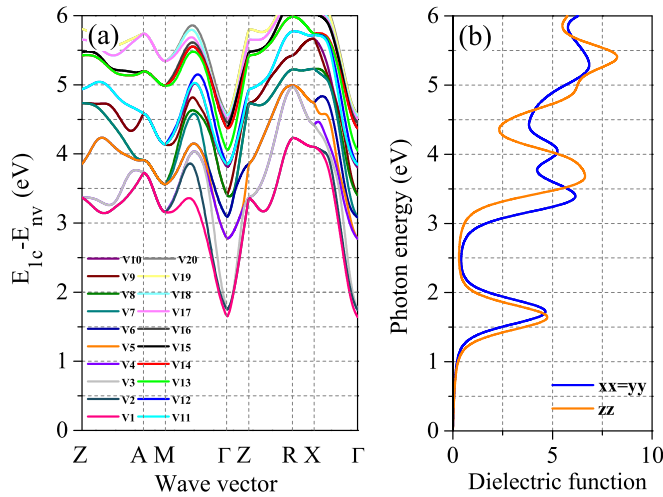
FIG. 8. (a) Joint band structure of chalcopyrite CuGaSe$_2$ along high symmetry points calculated using the HSE method, which shows the energy difference between the first conduction band and the top twenty valence bands. (b) Imaginary part of the dielectric function of chalcopyrite CuGaSe$_2$.

To reveal the effects of ordering parameter $\bar{\Pi}_{21}$ on electronic and optical properties, we simulated a partially disordered structure with desired $\bar{\Pi}_{21}$ by the SQS method. Experimentally, the synthesized solid solutions are usually partially disordered. Our simulations suggest that partially disordered CuGaSe$_2$ can be obtained by quenching above 700 K and that higher temperature introduces more disorder into this system. We constructed a partially disordered supercell of 64 atoms with nearly cubic lattice constants $a = b = 11.34$ Å, $c = 11.35$ Å. Figure 9(b) focuses on $\bar{\Pi}_{21} = -0.46$; the corresponding temperature is 2600 K, closer to the fully disordered phase (0). The perfect matching is obtained for $\bar{\Pi}_{21}$ after several iterations.

We adopted the SQS method to describe the fully disordered alloy, in which a small finite supercell is generated so that its averaged atomic correlation function $\bar{\Pi}_{km}$ is closest to the targeted correlation function $(2x - 1)^k$, where x is the alloy composition. We constructed tetragonal supercells of 64 and 128 atoms, respectively. $\bar{\Pi}_{km}$ of the pairs up to the fourth neighbor, the first-neighbored triangles and tetragons are all as the same as those of the fully disordered solid solution, and the detailed comparison is summarized in Table S6 in the SM for both systems. Comparing the energies of both supercells,
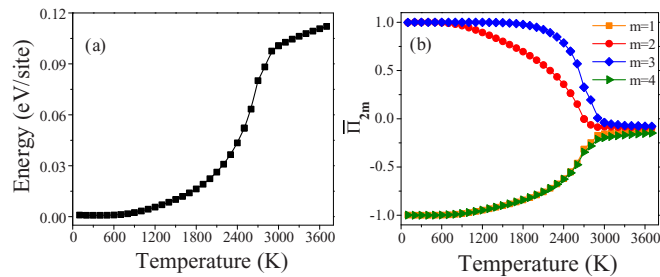

FIG. 9. (a) Monte Carlo simulation of the excess energy as a function of temperature and (b) the corresponding averaged atomic correlation functions of pairs up to the mth neighbor ($\bar{\Pi}_{2m}$).
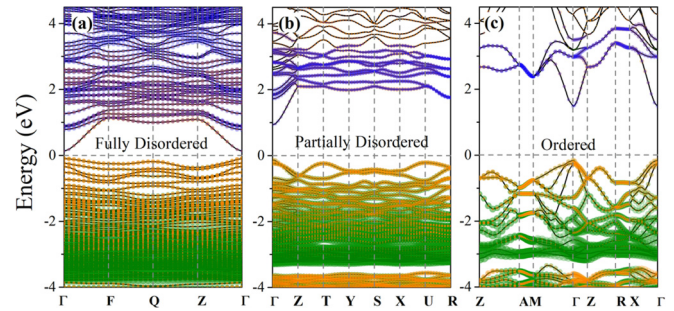

FIG. 10. HSE band structure of (a) fully disordered, (b) partially disordered, and (c) ordered CuGaSe$_2$. The yellow, green, and blue symbols represent Se p, Cu d, and Ga s orbitals, respectively. Different circle sizes correspond to the projected weights of different orbitals.

one finds that the 64-atom cell is energetically preferred to the 128-atom cell by 12.07 meV/atom; therefore, the 64-atom supercell is adopted to simulate the fully disordered structure, as well as the above partially disordered structure.

The band structures of the fully disordered, partially disordered, and ordered CuGaSe$_2$ are plotted together for comparison in Fig. 10, together with corresponding structural models shown in Fig. S9 in the SM. All the band gaps are direct with the VBM and CBM at the Γ point. As $\bar{\Pi}_{21}$ varies from -1 of the ordered phase to 0 of the fully disordered phase, the band gap of CuGaSe$_2$ is greatly reduced to 0.23 eV from 1.64 eV. Electronic band structure of the studied partially disordered phase with the band gap of ~ 1.06 eV is close to that of the ordered phase, with similar states near the VBM and CBM. Therefore, it is feasible to tune the band gap in these materials systems by introducing disorder into the alloy through appropriately controlling the synthesis temperature or annealing time. Figure 11 indicates that, for the fully disordered, partially disordered, and ordered CuGaSe$_2$, optical absorption thresholds are 0.033, 0.31, and 0.36 eV, which are significantly lower than band gaps of 0.23, 1.06, and 1.64 eV, respectively. This is a typical character of the direct band gap structure and the band gaps are responsible for the first peaks of light absorption. The visible- or infrared-light harvesting can be greatly enhanced because of the red shifts of absorption
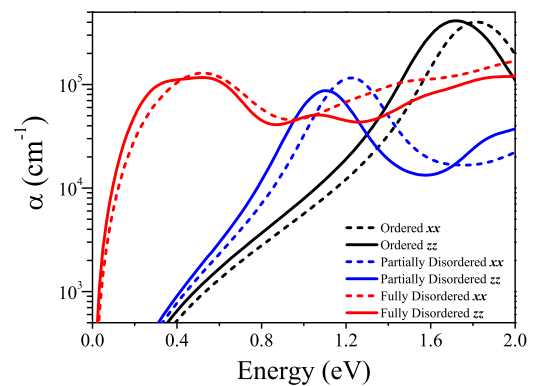

FIG. 11. Calculated optical absorption coefficients (α) of the ordered (black line), partially disordered (blue line), and fully disordered (red line) CuGaSe$_2$ using HSE functional.
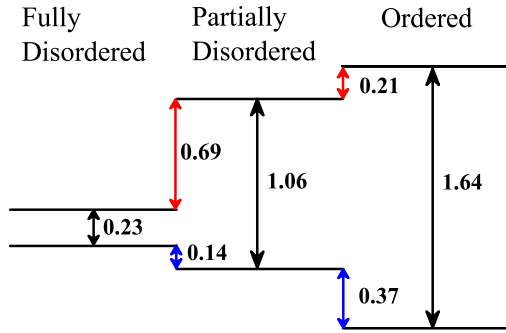
FIG. 12. Band alignment of the fully disordered, partially disordered, and ordered CuGaSe$_2$.

threshold with increasing degree of disorder, compared with the ordered phase.

The order-disorder phase diagram suggests that it is difficult to obtain fully disordered CuGaSe$_2$, which requires a quenching temperature above 2700 K due to the energy difference as large as 67.65 meV/atom between the fully disordered and the ordered phases. Reducing the transition temperature by p- or n-type doping has been theoretically proposed in the case of Cs$_2$AgBiBr$_6$ [25]. The band alignment of the fully disordered, partially disordered, and ordered CuGaSe$_2$ is plotted in Fig. 12. The valence-band offset ΔE_v is calculated following the same procedure as in the core-level photoemission measurement [69,70], where it is defined as

$$\Delta E_{\mathrm{v}} = \Delta E_{\mathrm{VBM,C}} - \Delta E_{\mathrm{VBM',C'}} + \Delta E_{\mathrm{C,C'}}. \qquad (4)$$

Here,

$$\Delta E_{\mathrm{VBM,C}} = E_{\mathrm{VBM}} - E_{\mathrm{C}} \qquad (5)$$

is the energy difference between the Se 1s core level and the VBM, and

$$\Delta E_{\mathrm{C,C'}} = E_{\mathrm{C}} - E_{\mathrm{C'}} \qquad (6)$$

is the difference in the Se 1s core level binding energy between two phases. The conduction-band offsets ΔE_c are depicted by adding the HSE band gaps to the valence-band offsets. When the degree of disorder is increased from the ordered phase to the fully disordered phase, the VBM rises by 0.51 eV, while the CBM drops by 0.90 eV. If extra holes are introduced to the VBM state, the fully disordered phase gains more energy than the ordered phase, so is that if extra electrons are introduced to the CBM state [25]. Therefore, it might be possible to reduce this energy difference and then the phase transition temperature of this alloy by n-type or p-type

doping. Furthermore, the band offset of the CBM (0.90 eV) is larger than that of the VBM (0.51 eV), thus the n-type doping would be more effective in reducing the transition temperature than the p-type doping.

V. CONCLUSIONS

In summary, we report on band gap engineering in Cu$_2$Se-Ga$_2$Se$_3$ alloys to improve the optoelectronic property. Using first-principles structural search, we identified the ground-state structures for Cu$_2$Se and Ga$_2$Se$_3$ whose total energies are slightly lower that those proposed previously. We also determined the stable phases for Cu$_4$Ga$_2$Se$_5$, CuGa$_3$Se$_5$, and CuGa$_5$Se$_8$ at ambient conditions, together with three high-pressure metallic phases for CuGaSe$_2$ and CuGa$_3$Se$_5$. These phases, phase transitions, and the distribution of cation-site vacancies are understood in terms of binding modes of Cu, Ga, and Se atoms. The computed electronic band structures indicate that these alloys all have direct band gaps varying from 0.77 eV (Cu$_4$Ga$_2$Se$_5$) to 2.11 eV (CuGa$_3$Se$_5$). The increased Ga composition cannot always enlarge the band gap; for example, the band gap of CuGa$_5$Se$_8$ is smaller than that of CuGa$_3$Se$_5$. This anomalous behavior of band structure can be explained by examining the p-d hybridization between Se and Cu atoms, which are tunable by Ga composition and pressure.

Furthermore, using Monte Carlo simulations and first-principles calculations, we show that, by introducing disorder to the cation sites of Cu and Ga in CuGaSe$_2$, the band gap can be engineered from 1.64 eV of the ordered phase to 0.23 eV of the fully disordered phase by controlling quenching temperature above 700 K, in order to facilitate light absorption in the visible and infrared regions. To synthesize such phases with desired absorption coefficients, it is necessary to reduce the temperature of order-disorder phase transition by p-type or n-type doping. Thus our study points to new possibilities of band gap engineering in copper gallium diselenides for potential technological applications.

[1] M. A. Contreras, K. Ramanathan, J. AbuShama, F. Hasoon, D. L. Young, B. Egaas, and R. Noufi, Prog. Photovoltaics **13**, 209 (2005).

[2] V. Koteski, S. Doka-Yamigno, J. Hofstetter, M. Rusu, H. E. Mahnke, M. C. Lux-Steiner, T. Schedel-Niedrig, and E. Arushanov, Phys. Rev. B **81**, 245213 (2010).

[3] E. Korhonen, K. Kuitunen, F. Tuomisto, A. Urbaniak, M. Igalson, J. Larsen, L. Gütay, S. Siebentritt, and Y. Tomm, Phys. Rev. B **86**, 064102 (2012).

[4] D. Barragan-Yani and K. Albe, Phys. Rev. B **95**, 115203 (2017).

[5] S. B. Zhang, S. H. Wei, and A. Zunger, Phys. Rev. Lett. **78**, 4059 (1997).

[6] N. Xiao, L. Zhu, K. Wang, Q. Dai, Y. Wang, S. Li, Y. Sui, Y. Ma, J. Liu, B. Liu, G. Zou, and B. Zou, Nanoscale **4**, 7443 (2012).

[7] M. Rusu, S. Wiesner, R. Wurz, S. Lehmann, S. D. Yamigno, A. Meeder, D. Marrón, M. Bär, V. Koteski, H. Mahnke, E. Arushanov, J. Beckmann, K. Höhn, W. Fritsch, W. Bohne, P. S. Bischoff, M. Heuken, A. J. Waldau, A. Rumberg, and T. S. Niedrig, Sol. Energ. Mat. Sol. C **95**, 1555 (2011).

[8] S. Wasim, C. Rincón, G. Marín, and J. Delgado, Appl. Phys. Lett. **77**, 94 (2000).

[9] S. Lehmann, D. Marrón, M. León, R. Feyerherm, E. Dudzik, E. Friedrich, M. Tovar, Y. Tomm, C. Wolf, S. Schorr, T. S. Niedrig, M. L. Steiner, and J. Merino, J. Appl. Phys. **109**, 013518 (2011).

[10] C. Rincón, S. M. Wasim, G. Marín, and I. Molina, J. Appl. Phys. **93**, 780 (2003).

[11] Y. Li, S. Wang, A. Oganov, H. Gou, J. Smith, and T. Strobel, Nat. Commun. **6**, 6974 (2015).

[12] W. Zhang, A. Oganov, A. Goncharov, Q. Zhu, S. Boulfelfel, A. Lyakhov, E. Stavrou, M. Somayazulu, V. Prakapenka, and Z. Konôpkovâ, Science **342**, 1502 (2013).

[13] H. Yu, W. Lao, L. Wang, K. Li, and Y. Chen, Phys. Rev. Lett. **118**, 137002 (2017).

[14] M. Zhang, H. Liu, Q. Li, B. Gao, Y. Wang, H. Li, C. Chen, and Y. Ma, Phys. Rev. Lett. **114**, 015502 (2015).

[15] C. Lu, M. Miao, and Y. Ma, J. Am. Chem. Soc **135**, 14167 (2013).

[16] Y. Ma, M. Eremets, A. Oganov, Y. Xie, I. Trojan, S. Medvedev, A. Lyakhov, M. Valle, and V. Prakapenka, Nature (London) **458**, 182 (2009).

[17] C. Zhao, Y. Duan, J. Gao, W. Liu, H. Dong, H. Dong, D. Zhang, and A. Oganov, Phys. Chem. Chem. Phys. **20**, 24665 (2018).

[18] A. Oganov, Faraday Discuss. **211**, 643 (2018).

[19] A. Kvashnin, H. Zakaryan, C. Zhao, Y. Duan, Y. Kvashnina, C. Xie, H. Dong, and A. Oganov, J. Phys. Chem. Lett. **9**, 3470 (2018).

[20] S. Chen, X. Gong, A. Walsh, and S. H. Wei, Appl. Phys. Lett. **94**, 041903 (2009).

[21] P. Newman, J. Phys. Chem. Solids **23**, 19 (1962).

[22] J. Ma, H. X. Deng, J. W. Luo, and S. H. Wei, Phys. Rev. B **90**, 115201 (2014).

[23] J. S. Park, J. H. Yang, A. Kanevce, S. Choi, I. L. Repins, and S. H. Wei, Phys. Rev. B **91**, 075204 (2015).

[24] D. Scanlon and A. Walsh, Appl. Phys. Lett. **100**, 251911 (2012).

[25] J. Yang, P. Zhang, and S. H. Wei, J. Phys. Chem. Lett. **9**, 31 (2018).

[26] A. Oganov, C. Pickard, Q. Zhu, and R. Needs, Nat. Rev. Mater. **4**, 331 (2019).

[27] D. de Fontaine, Solid State Phys. **47**, 33 (1994).

[28] F. Ducastelle, *Order and Phase Stability in Alloys* (North-Holland, Amsterdam, 1993).

[29] A. Oganov, Y. Ma, A. Lyakhov, M. Valle, and C. Gatti, Rev. Mineral. Geochem. **71**, 271 (2010).

[30] A. Oganov, A. Lyakhov, and M. Valle, Acc. Chem. Res. **44**, 227 (2011).

[31] A. Oganova and C. Glass, J. Chem. Phys. **124**, 244704 (2006).

[32] P. Hohenberg and W. Kohn, Phys. Rev. **136**, B864 (1964).

[33] W. Kohn and L. J. Sham, Phys. Rev. **140**, A1133 (1965).

[34] J. P. Perdew, K. Burke, and M. Ernzerhof, Phys. Rev. Lett. **77**, 3865 (1996).

[35] P. E. Blöchl, Phys. Rev. B **50**, 17953 (1994).

[36] G. Kresse and D. Joubert, Phys. Rev. B **59**, 1758 (1999).

[37] G. Kresse and J. Hafner, Phys. Rev. B **47**, 558 (1993).

[38] G. Kresse and J. Hafner, Phys. Rev. B **49**, 14251 (1994).

[39] G. Kresse and J. Furthmüller, Phys. Rev. B **54**, 11169 (1996).

[40] J. Heyd, G. E. Scuseria, and M. Ernzerhof, J. Chem. Phys. **118**, 8207 (2003).

[41] See Supplemental Material at http://link.aps.org/supplemental/10.1103/PhysRevMaterials.3.125405 for more details on the enthalpy differences, structural parameters, phonon spectrums, electronic band structures, convex hulls, band gaps, density of states, crystal structures, and elastic parameters.

[42] A. D. Becke and E. R. Johnson, J. Chem. Phys. **124**, 221101 (2006).

[43] G. P. Sorokin, Yu. M. Papshev, and P. T. Oush, Sov. Phys. Solid State **7**, 1810 (1966).

[44] G. Padam, Thin Solid Films **150**, L89 (1987).

[45] J. Shay, B. Tell, H. Kasper, and L. Schiavone, Phys. Rev. B **5**, 5003 (1972).

[46] M. A. Afifi, A. E. Bekheet, H. T. El-Shair, and I. T.Zedan, Physica B **325**, 308 (2003).

[47] S. H. Wei, L. G. Ferreira, and A. Zunger, Phys. Rev. B **41**, 8240 (1990).

[48] A. van de Walle, CALPHAD **33**, 266 (2009).

[49] K. Yamamoto and S. Kashida, J. Solid State Chem. **93**, 202 (1991).

[50] L. Gulay, M. Daszkiewicz, O. M. Strok, and A. Pietraszko, Chem. Met. Alloys **4**, 200 (2011).

[51] A. Jain, S. P. Ong, G. Hautier, W. Chen, W. D. Richards, S. Dacek, S. Cholia, D. Gunter, D. Skinner, G. Ceder, and K. A. Persson, APL Mater. **1**, 011002 (2013).

[52] G. L. W. Hart and R. W. Forcade, Phys. Rev. B **80**, 014120 (2009).

[53] Y. Zhang, X. Shao, Y. Zheng, L. Yan, P. Zhu, Y. Li, and H. Xu, J. Alloy. Compd. **732**, 280 (2018).

[54] H. Hahn and W. Klingler, Z. Anorg. Allg. Chem. **259**, 135 (1949).

[55] D. Lubbers and V. Leute, J. Solid State Chem. **43**, 339 (1982).

[56] S. Manna, P. Gorai, G. Brennecka, C. Ciobanu, and V. Stevanović, J. Mater. Chem. C **6**, 11035 (2018).

[57] Y. Duan, G. Tang, C. Chen, T. Lu, and Z. Wu, Phys. Rev. B **85**, 054108 (2012).

[58] J. E. Jaffe and A. Zunger, Phys. Rev. B **28**, 5822 (1983).

[59] J. E. Jaffe and A. Zunger, Phys. Rev. B **29**, 1882 (1984).

[60] A. Zunger, S.-H. Wei, L. G. Ferreira, and J. E. Bernard, Phys. Rev. Lett. **65**, 353 (1990).

[61] W. Yin, Y. Yan, and S. H. Wei, J. Phys. Chem. Lett. **5**, 3625 (2014).

[62] W. Sun, S. Dacek, S. P. Ong, G. Hautier, A. Jain, W. Richards, A. Gamst, K. Persson, and G. Ceder, Sci. Adv. **2**, e1600225 (2016).

[63] G. Marín, S. Wasim, C. Rincón, G. S. Pérez, P. Bocaranda, I. Molina, R. Guevara, and J. Delgado, J. Appl. Phys. **95**, 8280 (2004).

[64] M. Born and K. Huang, *Dynamical Theory of Crystal Lattices* (Oxford University Press, 1954).

[65] Y. Zhang, Y. Wang, L. Xi, R. Qiu, X. Shi, P. Zhang, and W. Zhang, J. Chem. Phys. **140**, 074702 (2014).

[66] Y. Duan, L. Qin, L. Shi, G. Tang, and H. Shi, Appl. Phys. Lett. **100**, 022104 (2012).

[67] J. Gao, Y. Duan, C. Zhao, W. Liu, H. Dong, D. Zhang, and H. Dong, J. Mater. Chem. C **7**, 1246 (2019).

[68] S.-H. Wei, L. G. Ferreira, J. E. Bernard, and A. Zunger, Phys. Rev. B **42**, 9622 (1990).

[69] S.-H. Wei and A. Zunger, J. Appl. Phys. **78**, 3846 (1995).

[70] S.-H. Wei and A. Zunger, Appl. Phys. Lett. **72**, 2011 (1998).